EPJ Web of Conferences **312**, 02007 (2024) https://doi.org/10.1051/epjconf/202431202007
FPCP 2024

Neutrino magnetic moment and inert doublet dark matter in a radiative seesaw scenario

Rukmani Mohanta[1,*], *Shivaramakrishna* Singirala[1,**], and *Dinesh* Singha[1,***]

[1]School of Physics, University of Hyderabad, Hyderabad - 500046, India

Abstract. We illustrate neutrino mass and magnetic moment along with dark matter phenomenology in a Type-III radiative scenario. To achieve this, we extend the Standard Model with three vector-like fermion triplets and two inert doublets, which can provide a suitable framework for studying the above phenomenological aspects. The inert scalars contribute to the total relic density of dark matter in the universe. The neutrino aspects are realized at one-loop level with magnetic moment obtained through charged scalars, while neutrino mass gets contribution from charged and neutral scalars. Taking inert scalar upto 2 TeV and triplet fermion mass in a few TeV range, we obtain a common parameter space, compatible with experimental limits associated with both neutrino and dark matter sectors. Finally, we demonstrate that the model is able to provide neutrino magnetic moments in a wide range from $10^{-12}\mu_B$ to $10^{-10}\mu_B$, meeting the bounds of various experiments such as Super-K, TEXONO, Borexino and XENONnT.

1 Introduction

Despite the overwhelming success of the Standard Model (SM) in accounting for the interactions among the elementary particles, it lacks the ability to explain the observed neutrino oscillation phenomenon as well as the dark matter content of the universe. Hence, the exploration of physics beyond the standard model becomes inevitable for the understanding of several open problems of nature. To accommodate the non-zero neutrino mass, many new ideas are put forward, which are expected to have implications in many other sectors. One such possibility amongst them is that neutrinos can possess electromagnetic properties like electric and magnetic dipole moments. Solar, accelerator and reactor experiments possibly could provide the direct measurement of magnetic moments and eventually put the limits on them.

In recent past, XENON collaboration performed a search for new physics with its 1 ton detector and reported an excess of events over the known backgrounds in the recoil energy range $1-7$ keV, peaked around 2.5 keV [1]. It turns out that such excess can be explained with large transition magnetic moment of neutrinos. With new data from its successor XENONnT [2], no visibly bold excess events were seen in the low energy region creating a bizarre situation between these two experiments. The collaboration is suspecting the excess in XENON1T

*e-mail: rmsp@uohyd.ac.in
**e-mail: krishnas542@gmail.com
***e-mail: dinesh.sin.187@gmail.com

was due to uncounted tritium whose presence or absence they can't corroborate. In this scenario, we cannot completely ignore the possible implication of new physics effects at XENON1T and that is why it is very interesting to explore such possibilities.

The nature and identity of dark matter remains still a mystery. Thus, we raise a question, whether a dark matter particle running in the loop, forming an electromagnetic vertex can provide neutrino magnetic moment. With this view point, we provide a simple model [3] that can accommodate non-zero magnetic moment for neutrino and also discuss dark matter phenomenology in a correlative manner.

The paper is organized as follows. In section-II, we describe the model along with the particle content and the relevant interaction terms to address neutrino magnetic moment, neutrino mass and dark matter. The mass spectrum of scalar sector due to mixing is also discussed in this section. Section-III narrates neutrino magnetic moment and neutrino masses at one-loop. Section-IV describes the dark matter relic density and its detection prospects. Section-V provides the detailed analysis, showing common parameter space to obtain observables related to the aspects of neutrino and dark matter sectors. Section-VI gives the signature of magnetic moment in the light of electron recoil event excess at XENON1T and also the overall obtained range of magnetic moment in the concerned model. Finally, concluding remarks are presented in section-VII.

2 Model description

To address the neutrino mass, magnetic moment and dark matter in a common platform, we extend the SM framework with three vector-like fermion triplets Σ_k, with $k = 1, 2, 3$ and two inert scalar doublets η_j, with $j = 1, 2$. We impose an additional Z_2 symmetry to realize neutrino phenomenology at one-loop and also for the stability of the dark matter candidate. The particle content along with their charges are displayed in Table. 1.

	Field	$SU(3)_C \times SU(2)_L \times U(1)_Y$	Z_2
Leptons	$\ell_L = (\nu, e)^T_L$	$(\mathbf{1}, \mathbf{2}, -1/2)$	+
	e_R	$(\mathbf{1}, \mathbf{1}, -1)$	+
	$\Sigma_{k(L,R)}$	$(\mathbf{1}, \mathbf{3}, 0)$	−
Scalars	H	$(\mathbf{1}, \mathbf{2}, 1/2)$	+
	η_j	$(\mathbf{1}, \mathbf{2}, 1/2)$	−

Table 1. Fields and their charges in the present model.

The $SU(2)_L$ triplet $\Sigma_{L,R} = \left(\Sigma^1, \Sigma^2, \Sigma^3\right)^T_{L,R}$ can be expressed in the fundamental representation as

$$\Sigma_{L,R} = \frac{\sigma^a \Sigma^a_{L,R}}{\sqrt{2}} = \begin{pmatrix} \Sigma^0_{L,R}/\sqrt{2} & \Sigma^+_{L,R} \\ \Sigma^-_{L,R} & -\Sigma^0_{L,R}/\sqrt{2} \end{pmatrix}. \tag{1}$$

Here, σ^a's represent Pauli matrices and $\Sigma^0_{L,R} = \Sigma^3_{L,R}$, $\Sigma^\pm_{L,R} = \left(\Sigma^1_{L,R} \mp \Sigma^2_{L,R}\right)/\sqrt{2}$. The relevant Lagrangian term involving the new particles of the model is given by

$$\mathcal{L}_\Sigma = y'_{\alpha k} \overline{\ell_{\alpha L}} \Sigma_{kR} \tilde{\eta}_j + y_{\alpha k} \overline{\ell^c_{\alpha L}} i\sigma_2 \Sigma_{kL} \eta_j + \frac{i}{2} \mathrm{Tr}[\overline{\Sigma} \gamma^\mu D_\mu \Sigma] - \frac{1}{2} \mathrm{Tr}[\overline{\Sigma} M_\Sigma \Sigma] + \text{h.c.}\,, \tag{2}$$

where $\Sigma^{+,0} = \Sigma_L^{+,0} + \Sigma_R^{+,0}$ and $\Sigma = (\Sigma_1, \Sigma_2, \Sigma_3)^T$. The covariant derivative for Σ is given by

$$D_\mu \Sigma = \partial_\mu \Sigma + ig \left[\sum_{a=1}^{3} \frac{\sigma^a}{2} W_\mu^a, \Sigma \right]. \tag{3}$$

The Lagrangian for the scalar sector takes the form

$$\mathcal{L}_{\text{scalar}} = \left| \left(\partial_\mu + \frac{i}{2} g\, \sigma^a W_\mu^a + \frac{i}{2} g' B_\mu \right) \eta_1 \right|^2 + \left| \left(\partial_\mu + \frac{i}{2} g\, \sigma^a W_\mu^a + \frac{i}{2} g' B_\mu \right) \eta_2 \right|^2 - V(H, \eta_1, \eta_2),$$

where, the inert doublets are denoted by $\eta_j = \left(\eta_j^+, \eta_j^0\right)^T$, with $\eta_j^0 = \dfrac{\eta_j^R + i\eta_j^I}{\sqrt{2}}$ and the scalar potential is expressed as [4]

$$\begin{aligned} V(H, \eta_1, \eta_2) = {} & \mu_H^2 H^\dagger H + \mu_1^2 \eta_1^\dagger \eta_1 + \mu_2^2 \eta_2^\dagger \eta_2 + \mu_{12}^2 (\eta_1^\dagger \eta_2 + \text{h.c}) + \lambda_H (H^\dagger H)^2 + \lambda_1 (\eta_1^\dagger \eta_1)^2 \\ & + \lambda_2 (\eta_2^\dagger \eta_2)^2 + \lambda_{12} (\eta_1^\dagger \eta_1)(\eta_2^\dagger \eta_2) + \lambda'_{12} (\eta_1^\dagger \eta_2)(\eta_2^\dagger \eta_1) + \frac{\lambda''_{12}}{2} \left[(\eta_1^\dagger \eta_2)^2 + \text{h.c.} \right] \\ & + \sum_{j=1,2} \left(\lambda_{Hj} (H^\dagger H)(\eta_j^\dagger \eta_j) + \lambda'_{Hj} (H^\dagger \eta_j)(\eta_j^\dagger H) + \frac{\lambda''_{Hj}}{2} \left[(H^\dagger \eta_j)^2 + \text{h.c} \right] \right). \end{aligned} \tag{4}$$

2.1 Mass spectrum

The mass matrices of the charged and neural scalar components are given by

$$\mathcal{M}_C^2 = \begin{pmatrix} \Lambda_{C1} & \mu_{12}^2 \\ \mu_{12}^2 & \Lambda_{C2} \end{pmatrix}, \quad \mathcal{M}_R^2 = \begin{pmatrix} \Lambda_{R1} & \mu_{12}^2 \\ \mu_{12}^2 & \Lambda_{R2} \end{pmatrix}, \quad \mathcal{M}_I^2 = \begin{pmatrix} \Lambda_{I1} & \mu_{12}^2 \\ \mu_{12}^2 & \Lambda_{I2} \end{pmatrix}, \tag{5}$$

where,

$$\Lambda_{Cj} = \mu_j^2 + \frac{\lambda_{Hj}}{2} v^2, \quad \Lambda_{(R/I)j} = \mu_j^2 + \left(\lambda_{Hj} + \lambda'_{Hj} \pm \lambda''_{Hj} \right) \frac{v^2}{2}. \tag{6}$$

One can diagonalize the above mass matrices using $U_\theta = \begin{pmatrix} \cos\theta & \sin\theta \\ -\sin\theta & \cos\theta \end{pmatrix}$ as

$$\begin{aligned} & U_{\theta_C}^T \mathcal{M}_C^2 U_{\theta_C} = \text{diag}(M_{C1}^2, M_{C2}^2) \quad \text{with} \quad \theta_C = \tan^{-1} \left[\frac{2\mu_{12}^2}{\Lambda_{C2} - \Lambda_{C1}} \right], \\ & U_{\theta_{R/I}}^T \mathcal{M}_{R/I}^2 U_{\theta_{R/I}} = \text{diag}(M_{(R/I)1}^2, M_{(R/I)2}^2) \quad \text{with} \quad \theta_{R/I} = \tan^{-1} \left[\frac{2\mu_{12}^2}{\Lambda_{(R/I)2} - \Lambda_{(R/I)1}} \right]. \end{aligned} \tag{7}$$

The flavor and mass eigen states can be related as

$$\begin{pmatrix} \eta_1^+ \\ \eta_2^+ \end{pmatrix} = U_{\theta_C} \begin{pmatrix} \phi_1^+ \\ \phi_2^+ \end{pmatrix}, \quad \begin{pmatrix} \eta_1^R \\ \eta_2^R \end{pmatrix} = U_{\theta_R} \begin{pmatrix} \phi_1^R \\ \phi_2^R \end{pmatrix}, \quad \begin{pmatrix} \eta_1^I \\ \eta_2^I \end{pmatrix} = U_{\theta_I} \begin{pmatrix} \phi_1^I \\ \phi_2^I \end{pmatrix}. \tag{8}$$

The invisible decays of Z and $W^\pm$ at LEP, limit the masses of inert scalars as [5, 6]

$$M_{Ci} > M_Z/2, \quad M_{Ri} + M_{Ii} > M_Z, \quad M_{Ci} + M_{Ri,Ii} > M_W. \tag{9}$$

Moving on to fermion sector, electroweak radiative corrections provide a mass splitting of 166 MeV [7] between the charged and neutral component of triplet. We work in the high scale regime, this small splitting does not effect the phenomenology.

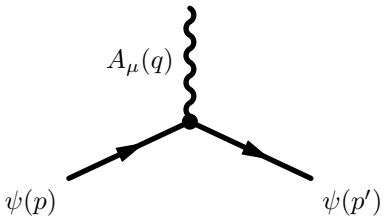

Figure 1. Effective electromagnetic vertex, where $q = p - p'$.

3 Neutrino phenomenology

3.1 Neutrino Magnetic moment

Though neutrino is electrically neutral, it can have electromagnetic interaction at loop level, as shown in Fig. 1, where the blob represents the effective one-loop coupling while $\psi(p)$ and $\psi(p')$ denote the incoming and outgoing neutrino states. The effective interaction Lagrangian takes the form

$$\mathcal{L}_{\rm EM} = \overline{\psi}\Gamma_\mu \psi A^\mu \ . \tag{10}$$

In the above, the electromagnetic vertex function varies with the type of neutrinos, i.e., Dirac or Majorana. In case of Dirac neutrino, Γ_μ takes the form

$$\Gamma_\mu(p,p') = f_Q(q^2)\gamma_\mu + i f_M(q^2)\sigma_{\mu\nu}q^\nu + f_E(q^2)\sigma_{\mu\nu}q^\nu\gamma_5 + f_A(q^2)(q^2\gamma_\mu - q_\mu q)\gamma_5 \ , \tag{11}$$

where $f_Q(q^2)$, $f_M(q^2)$, $f_E(q^2)$ and $f_A(q^2)$ represent the form factors of charge, magnetic dipole, electric dipole and anapole respectively.

In the non-relativisitic regime, $f_Q(0) = Q$ stands for the charge, $f_M(0) = \mu$ represents magnetic dipole moment, $f_E(0)$ denotes electric dipole moment and $f_A(0)$ stands for the Zeldovich anapole moment of the particle. All the four form factors remain finite in Dirac type neutrino. For Majorana case, using the property of charge conjugation $\psi^c = C\overline{\psi}^T$, we get

$$\overline{\psi}\Gamma_\mu\psi = \overline{\psi^c}\Gamma_\mu\psi^c = \overline{\psi}C\Gamma_\mu^T C^{-1}\psi. \tag{12}$$

Since $C\gamma_\mu^T C^{-1} = -\gamma_\mu$, $C(\gamma_\mu\gamma_5)^T C^{-1} = \gamma_\mu\gamma_5$, $C\sigma_{\mu\nu}^T C^{-1} = -\sigma_{\mu\nu}$ and $C(\sigma_{\mu\nu}\gamma_5)^T C^{-1} = -\sigma_{\mu\nu}\gamma_5$, we obtain

$$\Gamma_\mu(p,p') = -f_Q(q^2)\gamma_\mu - i f_M(q^2)\sigma_{\mu\nu}q^\nu - f_E(q^2)\sigma_{\mu\nu}q^\nu\gamma_5 + f_A(q^2)(q^2\gamma_\mu - q_\mu q)\gamma_5 \ , \tag{13}$$

which results $f_Q(q^2) = f_M(q^2) = f_E(q^2) = 0$ for a Majorana neutrino. However, if the electromagnetic current is between two different neutrino flavors in the initial and final states i.e., $\overline{\psi_i}\Gamma_\mu\psi_j A^\mu$ with $i \neq j$, Majorana neutrinos can have non-zero transition dipole moments.

In the present model, the magnetic moment arises from one-loop diagram shown in the left panel of Fig. 2, and the expression of corresponding contribution takes the form [3]

$$(\mu_\nu)_{\alpha\beta} = \sum_{k=1}^{3} \frac{(Y^2)_{\alpha\beta}}{8\pi^2} M_{\Sigma_k^+}\Bigg[(1+\sin 2\theta_C)\frac{1}{M_{C2}^2}\left(\ln\left[\frac{M_{C2}^2}{M_{\Sigma_k^+}^2}\right]-1\right)$$
$$+(1-\sin 2\theta_C)\frac{1}{M_{C1}^2}\left(\ln\left[\frac{M_{C1}^2}{M_{\Sigma_k^+}^2}\right]-1\right)\Bigg], \tag{14}$$

where $y = y' = Y$ and $(Y^2)_{\alpha\beta} = Y_{\alpha k}Y_{k\beta}^T$.

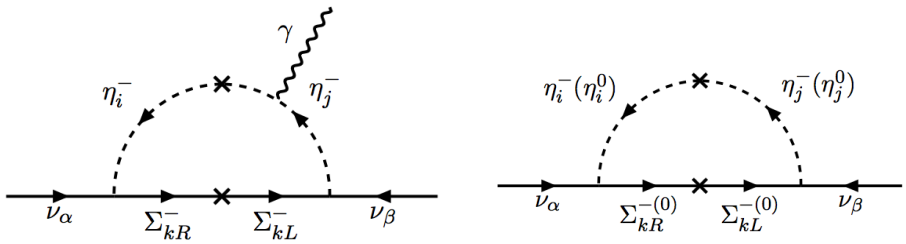

Figure 2. One-loop Feynman diagram for transition magnetic moment (left panel) and light neutrino mass (right panel).

3.2 Neutrino mass

In the present model, contribution to neutrino mass can arise at one-loop from two diagrams, one with charged scalars and fermion triplet in the loop while the other with neutral scalars and fermion triplets. The relevant diagrams are provided in the right panel of Fig. 2 and the corresponding contribution takes the form [3]

$$
\begin{aligned}
(\mathcal{M}_\nu)_{\alpha\beta} = &\sum_{k=1}^{3} \frac{(Y^2)_{\alpha\beta}}{32\pi^2} M_{\Sigma_k^+} \left[(1+\sin 2\theta_C) \frac{M_{C2}^2}{M_{\Sigma_k^+}^2 - M_{C2}^2} \ln\left(\frac{M_{\Sigma_k^+}^2}{M_{C2}^2}\right) + (1-\sin 2\theta_C) \frac{M_{C1}^2}{M_{\Sigma_k^+}^2 - M_{C1}^2} \ln\left(\frac{M_{\Sigma_k^+}^2}{M_{C1}^2}\right) \right] \\
&+ \sum_{k=1}^{3} \frac{(Y^2)_{\alpha\beta}}{32\pi^2} M_{\Sigma_k^0} \left[(1+\sin 2\theta_R) \frac{M_{R2}^2}{M_{\Sigma_k^0}^2 - M_{R2}^2} \ln\left(\frac{M_{\Sigma_k^0}^2}{M_{R2}^2}\right) + (1-\sin 2\theta_R) \frac{M_{R1}^2}{M_{\Sigma_k^0}^2 - M_{R1}^2} \ln\left(\frac{M_{\Sigma_k^0}^2}{M_{R1}^2}\right) \right] \\
&- \sum_{k=1}^{3} \frac{(Y^2)_{\alpha\beta}}{32\pi^2} M_{\Sigma_k^0} \left[(1+\sin 2\theta_I) \frac{M_{I2}^2}{M_{\Sigma_k^0}^2 - M_{I2}^2} \ln\left(\frac{M_{\Sigma_k^0}^2}{M_{I2}^2}\right) + (1-\sin 2\theta_I) \frac{M_{I1}^2}{M_{\Sigma_k^0}^2 - M_{I1}^2} \ln\left(\frac{M_{\Sigma_k^0}^2}{M_{I1}^2}\right) \right].
\end{aligned}
\tag{15}
$$

4 Dark Matter phenomenology

4.1 Relic density

In our proposed model, we consider the new scalar particles as dark matter candidates and study their phenomenology up to 2 TeV mass range. All the inert scalar components contribute to the dark matter relic density of the Universe through annihilations and co-annihilations. With the scalar Higgs mediator, $\phi_i^R \phi_j^R$ can annihilate to $f\bar{f}$, W^+W^-, ZZ, hh and via Z boson, $\phi_i^R \phi_j^I$ can co-annihilate to $f\bar{f}$, W^+W^-, Zh. Additionally, the charged and neutral components can co-annihilate to $f'\overline{f''}, AW^\pm, ZW^\pm, hW^\pm$ through $W^\pm$. Here, $f' = u, c, t, \nu_e, \nu_\mu, \nu_\tau$ and $f'' = d, s, b, e, \mu, \tau$. The abundance of dark matter can be computed using the stnadard formula,

$$
\Omega h^2 = \frac{1.07 \times 10^9 \text{ GeV}^{-1}}{M_{\text{Pl}}\, {g_*}^{1/2}} \frac{1}{J(x_f)} \,, \tag{16}
$$

where, $M_{\text{Pl}} = 1.22 \times 10^{19}$ GeV and $g_* = 106.75$ denote the Planck mass and total number of effective relativistic degrees of freedom respectively. The function J is defined by

$$
J(x_f) = \int_{x_f}^{\infty} \frac{\langle \sigma v \rangle(x)}{x^2} dx \,, \tag{17}
$$

where the thermally averaged cross section $\langle\sigma v\rangle$ reads as

$$\langle\sigma v\rangle(x) = \frac{x}{8M_{\rm DM}^5 K_2^2(x)} \int_{4M_{\rm DM}^2}^{\infty} \hat{\sigma} \times (s - 4M_{\rm DM}^2)\ \sqrt{s}\ K_1\left(\frac{x\sqrt{s}}{M_{\rm DM}}\right) ds. \tag{18}$$

Here K_1, K_2 are the modified Bessel functions, $x = M_{\rm DM}/T$, with T being the temperature, $M_{\rm DM}$ is dark matter mass, $\hat{\sigma}$ is the dark matter cross section and x_f stands for the freeze-out parameter.

4.2 Direct searches

The direct search signals come from the scattering off the scalar dark matter from the nucleus via the Higgs and the Z boson. Mass splitting between real and imaginary components above 100 KeV can forbid gauge kinematics [8]. Thus, the DM-nucleon cross section in Higgs portal can provide a spin-independent (SI) cross section, whose sensitivity can be checked with stringent upper bound of LZ-ZEPLIN experiment. The effective interaction Lagrangian in Higgs portal takes the form

$$\mathcal{L}_{\rm eff} = a_q \phi_1^R \phi_1^R q\overline{q}, \quad \text{where} \tag{19}$$

$$a_q = \frac{M_q}{2M_h^2 M_{R1}}(\lambda_{L1}\cos^2\theta_R + \lambda_{L2}\sin^2\theta_R) \text{ with } \lambda_{Lj} = \lambda_{Hj} + \lambda'_{Hj} + \lambda''_{Hj}.$$

The corresponding cross section is given by [8],

$$\sigma_{\rm SI} = \frac{1}{4\pi}\left(\frac{M_n M_{R1}}{M_n + M_{R1}}\right)^2 \left(\frac{\lambda_{L1}\cos^2\theta_R + \lambda_{L2}\sin^2\theta_R}{2M_{R1}M_h^2}\right)^2 f^2 M_n^2, \tag{20}$$

where, M_n denotes the nucleon mass, nucleonic matrix element $f \sim 0.3$. We have used micrOMEGAs to compute relic density and also DM-nucleon cross section. The detailed analysis of neutrino and dark matter observables and their viability through a common parameter space will be discussed in the next section.

5 Analysis

In the present framework, we consider ϕ_1^R to be the lightest inert scalar eigen state and there are five other heavier scalars. To make the analysis simpler, we consider the mass parameters related to the scalar masses as follows: one parameter M_{R1} corresponding to the mass of ϕ_1^R and three mass splittings namely δ, $\delta_{\rm IR}$ and $\delta_{\rm CR}$. The masses of the rest of the inert scalars can be derived using the following relations:

$$\begin{aligned} &M_{R2} - M_{R1} = M_{I2} - M_{I1} = M_{C2} - M_{C1} = \delta, \\ &M_{Ri} - M_{Ii} = \delta_{\rm IR}, \quad M_{Ri} - M_{Ci} = \delta_{\rm CR}\ , \end{aligned} \tag{21}$$

where, $i = 1, 2$. In the above set up, the scalar mixing angles can be related as follows

$$\sin 2\theta_I = \sin 2\theta_R \left(\frac{2M_{R1} + \delta}{2M_{R1} + 2\delta_{\rm IR} + \delta}\right), \qquad \sin 2\theta_C = \sin 2\theta_R \left(\frac{2M_{R1} + \delta}{2M_{R1} + 2\delta_{\rm CR} + \delta}\right). \tag{22}$$

We have performed the scan over model parameters as given below, in order to obtain the region, consistent with experimental bounds associated with both dark matter and neutrino sectors:

$$\begin{aligned} &100\ {\rm GeV} \le M_{R1} \le 2000\ {\rm GeV}, \quad 0 \le \sin\theta_R \le 1, \\ &0.1\ {\rm GeV} \le \delta < 200\ {\rm GeV}, \quad 0.1\ {\rm GeV} \le \delta_{\rm IR}, \delta_{\rm CR} \le 20\ {\rm GeV}. \end{aligned} \tag{23}$$

We filter out the parameter space by providing Planck constraint on relic density [9] in 3σ and then compute DM-nucleon SI cross section for the available parameter space. We project the cross section as a function of M_{R1} in the left panel of Fig. 3 with cyan data points, where the dashed brown line corresponds to LZ-ZEPLIN upper limit [10]. Choosing a set of values for the Yukawa and fermion triplet mass, with the obtained parameter space, one can satisfy the aspects of neutrino mass and mixing phenomenology. The blue, green and red data points corresponding to 25, 80 and 420 TeV of triplet mass and suitable Yukawa satisfy the neutrino magnetic moment and light neutrino mass in the desired range simultaneously, as projected in the right panel. We notice that a wide region of dark matter mass is favoured as we move towards high scale (triplet mass) and moreover the favourable region shifts towards larger values with scale. The suitable region of Yukawa and fermion triplet mass is depicted in the left panel of Fig. 4, allowed range for scalar mass splittings is displayed in the right panel. Here light colored band corresponds to $\delta_{\rm IR}$ and dark colored band stands for $\delta_{\rm CR}$. Using two

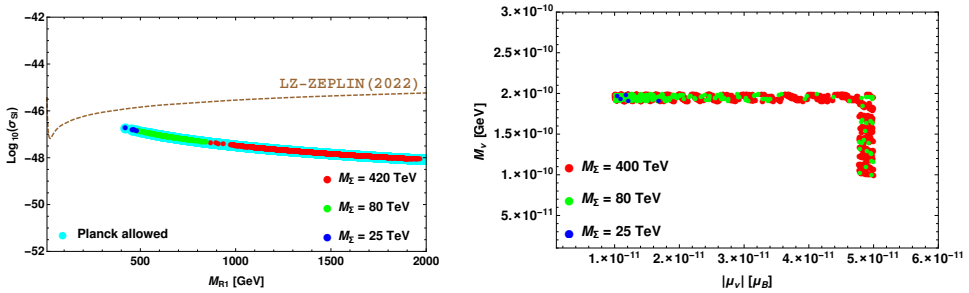

Figure 3. Left panel projects SI WIMP-nucleon cross section as a function M_{R1}, with dashed brown line of LZ-ZEPLIN upper limit [10]. Cyan data points satisfy Planck limit [9] on relic abundance in 3σ. Blue, green and red data points satisfy neutrino mass and magnetic moment for a specific set of values for fermion triplet and Yukawa, visible in the right panel.

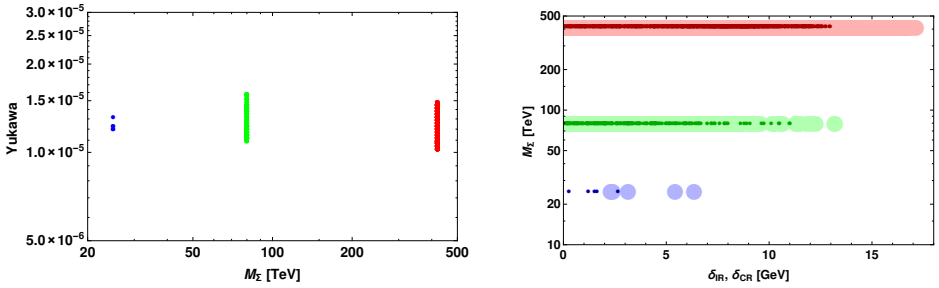

Figure 4. Left panel displays the suitable region for triplet mass and Yukawa to explain neutrino phenomenology. Right panel shows the allowed region for scalar mass splittings, thick (thin) bands correspond to $\delta_{\rm IR}(\delta_{\rm CR})$ respectively.

specific benchmark values (shown in table. 2 and table. 3) which are favourable to explain both neutrino and dark matter aspects discussed so far, we project relic abundance scalar dark matter in Fig. 5.

Table 2. Set of benchmarks from the consistent parameter space.

	M_{R1} [GeV]	δ [GeV]	$\delta_{\rm CR}$ [GeV]	$\delta_{\rm IR}$ [GeV]	M_Σ [TeV]	Yukawa	$\sin\theta_R$
benchmark-1	1472	101.69	9.03	0.35	420	$10^{-4.89}$	0.09
benchmark-2	628	36.40	4.38	3.45	80	$10^{-4.85}$	0.06

Table 3. Neutrino and dark matter observables for the given benchmarks.

	$\lvert\mu_\nu\rvert$ [μ_B]	$\mathcal{M}_\nu$ [GeV]	$\text{Log}_{10}^{[\sigma_{\rm SI}]}$ cm^{-2}	Ωh^2
benchmark-1	2.73×10^{-11}	1.99×10^{-10}	−47.78	0.123
benchmark-2	3.03×10^{-11}	1.92×10^{-10}	−47.04	0.119

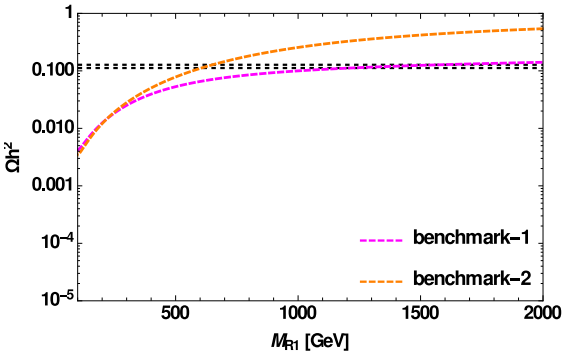

Figure 5. Relic density as a function of dark matter mass for the chosen benchmark of the favourable parameter space of table-2.

6 Implications

In the experimental perspective, non-zero neutrino magnetic moment of solar neutrinos can provide explanation for the excess in electron recoil events at XENON1T collaboration [1]. In other words, the neutrino transition magnetic moment can provide additional contribution to the neutrino-electron scattering process. In this section, we utilize non-zero transition neutrino magnetic moment to explain the excess in electron recoil events.

In the presence of magnetic moment, the total differential cross section can be given as

$$\left(\frac{d\sigma}{dT_e}\right)_{\rm TOT} = \left(\frac{d\sigma}{dT_e}\right)_{\rm SM} + \left(\frac{d\sigma}{dT_e}\right)_{\rm EM}, \tag{24}$$

where T_e is the electron recoil energy. The first contribution in eq. (24) is due to standard weak interactions, given by

$$\left(\frac{d\sigma}{dT_e}\right)_{\rm SM} = \frac{G_F^2 m_e}{2\pi}\left[(g_V+g_A)^2 + \left(1-\frac{T_e}{E_\nu}\right)^2(g_V-g_A)^2 + \left(\frac{m_e T_e}{E_\nu^2}\right)(g_A^2-g_V^2)\right], \tag{25}$$

where G_F stands for the Fermi constant and

$$g_V = 2\sin^2\theta_W + \frac{1}{2}, \quad g_A = 1/2 \text{ for } \nu_e,$$
$$g_V = 2\sin^2\theta_W - \frac{1}{2}, \quad g_A = -1/2 \text{ for } \nu_\mu, \nu_\tau \,. \tag{26}$$

The second contribution comes from the effective electromagnetic vertex of the neutrinos, i.e., magnetic moment contribution, which is expressed as

$$\left(\frac{d\sigma}{dT_e}\right)_{\rm EM} = \frac{\pi\alpha^2}{m_e^2}\left(\frac{1}{T_e} - \frac{1}{E_\nu}\right)\left(\frac{\mu_{\nu_{e\mu}}}{\mu_B}\right)^2, \tag{27}$$

where, α is the electromagnetic coupling, E_ν is the initial neutrino energy, $\mu_{\nu_{e\mu}}$ is the neutrino magnetic moment and μ_B is the Bohr magneton. For high T_e value, weak cross-section dominates and for low T_e value, the electromagnetic cross-section dominates and hence, we search for the signature of neutrino magnetic moment in the low energy region. For simplicity, we take one transition magnetic moment $\mu_{\nu_{e\mu}}$ to explain the XENON1T excess. The differential event rate to estimate the XENON1T signal is given by

$$\frac{dN}{dT_r} = n_{\rm te} \times \int_{E_\nu^{\rm min}}^{E_\nu^{\rm max}} dE_\nu \int_{T_{\rm th}}^{T_{\rm max}} dT_e \left(\frac{d\sigma^{\nu_e e}}{dT_e}P_{ee} + \cos^2\theta_{23}\frac{d\sigma^{\nu_\mu e}}{dT_e}P_{e\mu}\right) \times \frac{d\phi_s}{dE_\nu} \times \epsilon(T_e) \times G(T_e, T_r). \tag{28}$$

In the above, $\epsilon(T_e)$ denotes the efficiency of detector [1], n_{te} is the count of number of target electrons in the fiducial volume of one ton Xenon [11], $d\phi_s/dE_\nu$ represents the solar neutrino flux spectrum [12], and the function $G(T_e, T_r)$ reflects the normalised Gaussian smearing function that takes into account the detector's limited energy resolution [1]. The limits $T_{\rm th} = 1$ KeV and $T_{\rm max} = 30$ KeV stand for the threshold and maximum recoil energy of detector respectively. The extremes of neutrino energy for the integral are given by $E_\nu^{\rm max} = 420$ KeV and $E_\nu^{\rm min} = [T + (2m_e T + T^2)^{\frac{1}{2}}]/2$ [13]. The survival probability can be expressed as

$$P_{ee} = \sin^4\theta_{13} + \frac{1}{2}\cos^4\theta_{13}(1 + \cos 2\theta_{12}^m + \cos 2\theta_{12}) \,. \tag{29}$$

And the disappearance probability can be taken as $P_{e\mu/\tau} = 1 - P_{ee}$. The oscillation parameters are taken from [14]. In Fig. 6, we project the event rate as a function of recoil energy T_r, for two set of values for magnetic moment, i.e., $\mu_{\nu_{e\mu}} = 2.6 \times 10^{-11}\mu_B$ and $3.2 \times 10^{-11}\mu_B$ (red curves). Adding with the background (green curve), we are able to meet the observed recoil event excess in the low energy region near 2.5 KeV as of XENON1T experiment [1]. In Fig. 7, we project neutrino magnetic moment as a function of dark matter mass, choosing specific set of values assigned to triplet fermion. As seen earlier in the left panel of Fig. 3, a specific range of dark matter mass is favoured with the scale of triplet mass. It is transparent that the model parameters are able to provide neutrino magnetic moment in the range $10^{-12}\mu_B$ to $10^{-10}\mu_B$, sensitive to the upper limits of Super-K [15], TEXONO [16], Borexino [17], XENON1T [1], XENONnT [2] and white dwarfs [18] (colored horizontal lines). Thus, from all the above discussions made, it is evident that this simple framework can provide a consistent phenomenological platform for a correlative study of neutrino magnetic moment (especially), mass and dark matter physics.

7 Conclusions

In this work, we have attempted to address neutrino mass, magnetic moment and dark matter phenomenology in a common framework. For this purpose, we have extended the standard

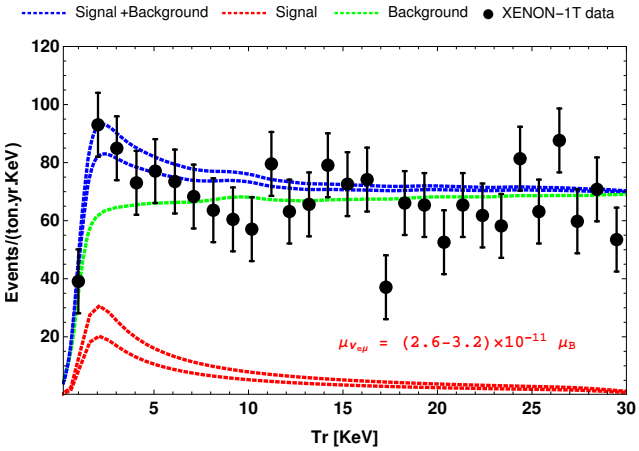

Figure 6. Excess recoil events (blue) to match XENON1T [1] (black) through the signal from transition neutrino magnetic moment $\mu_{\nu_{e\mu}} = 2.6 \times 10^{-11}\mu_B$ and $3.2 \times 10^{-11}\mu_B$ (in red) along with background (green).

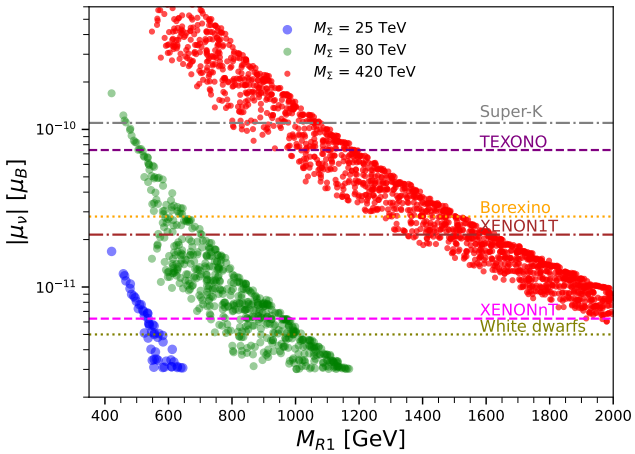

Figure 7. Allowed region of neutrino magnetic moment with the mass spectrum of dark matter and fermion triplet. Horizontal colored lines stand for the upper bounds of XENON1T (average value of suggested range in [1]), XENONnT [2], Borexino [17], TEXONO [16], Super-K [15] and white dwarfs [18].

model with three vector-like fermion triplets and two inert scalar doublets to realize Type-III radiative scenario. A pair of charged scalars help in obtaining neutrino magnetic moment, all charged and neutral scalars come up in getting light neutrino mass at one-loop level. All the inert scalars participate in annihilation and co-annihilation channels to provide total dark matter relic density of the Universe, consistent with Planck satellite data and also provide a suitable cross section with nucleon, sensitive to LZ-ZEPLIN upper limit. The lightest dark matter mass is scanned upto 2 TeV while the fermion triplet mass is taken with larger values, i.e., few hundred TeV. Choosing Yukawa of the order 10^{-5}, we have obtained light neutrino

mass in sub-eV scale and also transition magnetic moment $\sim 10^{-11}\,\mu_B$, to successfully explain the excess electron recoil events at low energy scale reported by XENON1T experiment. Finally, we have also demonstrated with a plot that the model is able to provide neutrino magnetic moment in a wide range ($10^{-12}\mu_B$ to $10^{-10}\mu_B$), in the same ball park of Borexino, Super-K, TEXONO, XENONnT and white dwarfs. Overall, this simple model provides a suitable platform to study neutrino phenomenology, especially the neutrino magnetic moment and also dark matter aspects.

Acknowledgments

RM would like to acknowledge University of Hyderabad IoE project grant no. RC1-20-012.

References

[1] E. Aprile et al. [XENON Collaboration], Excess electronic recoil events in XENON1T, Phys. Rev. D **102**, 072004 (2020). https://doi.org/10.1103/PhysRevD.102.072004

[2] E. Aprile et al. [XENON Collaboration], Search for New Physics in Electronic Recoil Data from XENONnT, Phys. Rev. Lett. **129**, 161805 (2022). https://doi.org/10.1103/PhysRevLett.129.161805

[3] S. Singirala, D. K. Singha, R. Mohanta, Neutrino magnetic moment and inert doublet dark matter in a Type-III radiative scenario, Phys. Rev. D **108**, 095048 (2023). https://doi.org/10.1103/PhysRevD.108.095048

[4] V. Keus, S. F. King, S. Moretti, D. Sokolowska, Dark Matter with Two Inert Doublets plus one Higgs Doublet, JHEP **11**, 016 (2014). https://doi.org/10.1007/JHEP11(2014)016

[5] Q-H. Cao, E. Ma, G. Rajasekaran, Observing the Dark Scalar Doublet and its Impact on the Standard-Model Higgs Boson at Colliders, Phys. Rev. D **76**, 095011 (2007). https://doi.org/10.1103/PhysRevD.76.095011

[6] E. Lundstrom, M. Gustafsson, J. Edsjo, The Inert Doublet Model and LEP II Limits, Phys. Rev. D **79**, 035013 (2009). https://doi.org/10.1103/PhysRevD.79.035013

[7] M. Cirelli, N. Fornengo, A. Strumia, Minimal Dark Matter, Nucl. Phys. B. **753**, 178 (2006). https://doi.org/10.1016/j.nuclphysb.2006.07.012

[8] E. Lundstrom, E. M. Dolle, S. Su, The Inert Dark Matter, Phys. Rev. D **80**, 055012 (2009). https://doi.org/10.1103/PhysRevD.80.055012

[9] N. Aghanim et al [Planck Collaboration], Planck 2018 results. VI. Cosmological parameters, Astron. Astrophys. **641**, A6 (2020). https://doi.org/10.1051/0004-6361/201833910

[10] J. Aalbers et al. [LZ Collaboration], First Dark Matter Search Results from the LUX-ZEPLIN (LZ) Experiment, Phys. Rev. Lett. **131**, 041002 (2022). https://doi.org/10.1103/PhysRevLett.131.041002

[11] E. Aprile et al. [XENON Collaboration], Energy resolution and linearity of XENON1T in the MeV energy range, Eur. Phys. J. C. **80**, 785 (2020). https://doi.org/10.1140/epjc/s10052-020-8284-0

[12] J. N. Bahcall, C. Pena-Garay, Solar models and solar neutrino oscillations, New. J. Phys. **6**, 63 (2004). https://doi.org/10.1088/1367-2630/6/1/063

[13] K. S. Babu, S. Jana, M. Lindner, Large Neutrino Magnetic Moments in the Light of Recent Experiments, JHEP **10**, 140 (2020). https://doi.org/10.1007/JHEP10(2020)040

[14] E. Esteban et al, Large Neutrino Magnetic Moments in the Light of Recent Experiments, JHEP **09**, 178 (2020). https://doi.org/10.1007/JHEP09(2020)178

[15] D. W. Liu et al. [Super-Kamiokande Collaboration], Limits on the neutrino magnetic moment using 1496 days of Super-Kamiokande-I solar neutrino data, Phys. Rev. Lett. **93**, 021802 (2004). https://doi.org/10.1103/PhysRevLett.93.021802

[16] H. T. Wong et al. [TEXONO Collaboration], A Search of Neutrino Magnetic Moments with a High-Purity Germanium Detector at the Kuo-Sheng Nuclear Power Station, Phys. Rev. D **75**, 012001 (2007). https://doi.org/10.1103/PhysRevD.75.012001

[17] M. Agostini et al. [Borexino Collaboration], Limiting neutrino magnetic moments with Borexino Phase-II solar neutrino data, Phys. Rev. D **96**, 091103 (2017). https://doi.org/10.1103/PhysRevD.96.091103

[18] M. Miguel Miller, Limits on the neutrino magnetic dipole moment from the luminosity function of hot white dwarfs, Astron.Astrophys. **562**, A123 (2014). https://doi.org/10.1051/0004-6361/201322641